The Influence of Particulates on Thruster Plume / Shock Layer Interaction at High Altitudes

Sergey F. Gimelshein and Alina A. Alexeenko
University of Southern California, Los Angeles, CA 90089

Dean C. Wadsworth and Natalia E. Gimelshein
ERC, Inc., Edwards AFB, CA 93524

Abstract

A two-phase plume flow from a small aluminized propellant side thruster interacting with rarefied atmosphere at 120 km has been examined numerically. A three step continuum-kinetic approach has been used, with the Navier-Stokes equations solved inside the nozzle, and a 2D/3D DSMC method employed to compute the plume nearfield and then the plume-atmosphere interaction region. At each of these steps, a two-way gas-particulate coupling has been used. The DSMC implementation uses molecular fluxes to calculate the number of gas-particulate collisions, and is based on a statistical approach to calculate deflection angles. A sensitivity study of various parameters of the approach is performed. The importance of two-way coupling, particle radiative cooling, and molecule accommodation on particle surface are analyzed.

1 Introduction

The combustion and relaxation processes in rocket propulsion systems result in the formation of particulates of different size and nature. Aluminum oxide particles, associated with all types of aluminized propellants, compose up to 30% of the exhaust mass fraction and may significantly impact both the gas flow inside the nozzle and plume-atmosphere interaction phenomena. Unburnt drops of liquid propellants are another important class of particles. Although large in size, they do not affect the bulk gas flow due to their small mass fractions; they may, however, cause significant contamination problems. Soot must also be considered for liquid propellant thrusters; these particulates are not expected to significantly impact the gas flow properties, but are important contributors to plume radiation signature.

Significant efforts have been made in the aerospace community toward accurate prediction of aluminum oxide particle impact on thruster performance and exhaust plume structure (see, for example, [1]). Many of the numerical efforts however were limited to low-altitude, high ambient density flow regimes. The continuum CFD based approaches can not be used to model the influence of particulates on the plume-atmosphere interaction at high altitudes, where the flow nonequilibrium is too strong and these approaches become unsuitable. A kinetic approach, such as the direct simulation Monte Carlo (DSMC) method, has to be used to obtain credible information on these flows.

The main objectives of this work are to compare gas-only and two-phase steady-state three-dimensional DSMC predictions of the flowfield surrounding a small side-mounted solid propellant attitude control thruster at high altitudes, and to assess the impact of particles on shock layer structure and plume observables. To the best of our knowledge, this work is the first application of the DSMC method to model full 3D two-phase plume-atmosphere interaction. Special attention is paid to the influence of different simulation parameters and flow phenomena, such as one- or two-way coupling, gas-particulate interactions, and particle radiation cooling, on gas and particulate density and temperature distributions. The present study focuses on a flow from a 130 N aluminized propellant thruster into atmosphere at an altitude of 120 and a free stream speed of 5 km/s.

Large particle loadings for the cases under consideration prevent the application of a simple overlay particle tracking approach and a two-way coupling needs to be used. The first implementation of a two-way coupling in the DSMC method was presented in [2]. The approach proposed in this work is different from [2], and the details of the present approach are given below. Similar to [2], the model [3] was used to sim-

Report Documentation Page

Form Approved
OMB No. 0704-0188

1. REPORT DATE	2. REPORT TYPE	3. DATES COVERED
JAN 2005		**-**

4. TITLE AND SUBTITLE	5a. CONTRACT NUMBER
The Influence of Particulates on Thruster Plume / Shock Layer Interaction at High Altitudes	5b. GRANT NUMBER
	5c. PROGRAM ELEMENT NUMBER
6. AUTHOR(S)	5d. PROJECT NUMBER
Sergey Gimelshein; Alina Alexeenko; Natalia Gimelshein; Dean Wadsworth	**5503**
	5e. TASK NUMBER **000P**
	5f. WORK UNIT NUMBER
7. PERFORMING ORGANIZATION NAME(S) AND ADDRESS(ES)	8. PERFORMING ORGANIZATION REPORT NUMBER
Air Force Research Laboratory (AFMC),AFRL/PRSA,10 E. Saturn Blvd.,Edwards AFB,CA,93524-7680	
9. SPONSORING/MONITORING AGENCY NAME(S) AND ADDRESS(ES)	10. SPONSOR/MONITOR'S ACRONYM(S)
	11. SPONSOR/MONITOR'S REPORT NUMBER(S)

12. DISTRIBUTION/AVAILABILITY STATEMENT

Approved for public release; distribution unlimited

13. SUPPLEMENTARY NOTES

14. ABSTRACT

A two-phase plume flow from a small aluminized propellant side thruster interacting with rarefied atmosphere at 120 km has been examined numerically. A three step continuum-kinetic approach has been used, with the Navier-Stokes equations solved inside the nozzle, and a 2D/3D DSMC method employed to compute the plume nearfield and then the plume-atmosphere interaction region. At each of these steps, a two-way gas-particulate coupling has been used. The DSMC implementation uses molecular fluxes to calculate the number of gas-particulate collisions, and is based on a statistical approach to calculate deflection angles. A sensitivity study of various parameters of the approach is performed. The importance of two-way coupling, particle radiative cooling, and molecule accommodation on particle surface are analyzed.

15. SUBJECT TERMS

16. SECURITY CLASSIFICATION OF:			17. LIMITATION OF ABSTRACT	18. NUMBER OF PAGES	19a. NAME OF RESPONSIBLE PERSON
a. REPORT	b. ABSTRACT	c. THIS PAGE			
unclassified	**unclassified**	**unclassified**		**12**	

ulate the impact of gas molecules on aluminum oxide particulates. The current algorithm does not use an analytic approximation for the molecule deflection angle, but implements an approach based on a statistical determination of the reflection point, and reflection procedure in accordance with the Maxwell model with specified tangential and energy accommodation coefficients. The molecule-particle collision rate is based on the particle number flux values, and not on the NTC scheme. All energies (translational and internal) of molecules are included in the energy transfer, and the Maxwell diffuse-specular model is used to calculate after-collision molecular states. The proposed procedure has linear dependence of computational time on the number of molecules and particles.

2 General modeling strategy

The modeling of the plume-atmosphere interaction is performed in three steps. First, the VIPER two-phase CFD code [4, 5] is utilized to obtain the solutions inside the nozzle. The VIPER solution at the nozzle exit is then used as the inflow boundary condition for an axisymmetric DSMC computation of the plume near field. As a result of the second step, a starting surface for a subsequent 3D DSMC computation is available at a distance from the exit were the plume density is too high for the ambient atmosphere to have any noticeable impact on the plume. The third step is full 3D DSMC modeling of the plume - atmosphere interaction that also includes chemical reactions between gas species. SMILE [6] DSMC-based computational tool is used for the second and third steps, extended to include particulates coupled with the gas flow. All three stages incorporate a two-way coupling between gas molecules and alumina particles.

2.1 VIPER code

VIPER[4, 5] is an axisymmetric Parabolized Navier-Stokes (PNS) code that includes finite rate gas chemistry, multiphase capability (via a two-way coupled Lagrangian method), and a variety of mostly empirical models for gas-particulate interaction and particulate evolution phenomena. The PNS scheme is applied from the sonic line near the throat to the nozzle exit plane. Separate methods are provided to model the combustion chamber and converging section. The combustion chamber pressure and temperature were assumed to be 3.85 atm and 2900 K, respectively. These conditions result in an exit plane gas pressure of approximately one percent of one atmosphere, and are essentially the lower limits for which a successful VIPER run could be made. Under these conditions, it is expected that the VIPER results give a qualitative, rather than quantitative, prediction of the 2-phase nozzle flow, suitable for engineering studies.

2.2 SMILE code

The 2D/3D DSMC-based code SMILE [6] has been used as the principal kinetic approach. The important features of SMILE that are relevant to this work are parallel capability, different collision and macroparameter grids with manual and automatic adaptations, and spatial weighting for axisymmetric flows.

The majorant frequency scheme [7] was used to calculate intermolecular interactions. The intermolecular potential was assumed to be a variable hard sphere [8]. Energy redistribution between the rotational and translational modes was performed in accordance with the Larsen-Borgnakke model. The total collision energy model [8] was used to model chemical reactions in gas. Species weights were used for particulate species. A temperature-dependent rotational relaxation number was used. The reflection of molecules on the nozzle and rocket surface was assumed to be diffuse with complete energy and momentum accommodation. An extension of SMILE to simulate two-phase flows is discussed in the following section.

3 DSMC implementation details

The present DSMC implementation uses the following assumptions: (i) particulates are spherical, and their rotation does not impact the flow, (ii) particulates are uniform, and have no internal temperature gradients, and (iii) the gas mean free path is larger than the particle diameter, so the gas flow is essentially free-molecular with regard to particle sizes. This means that there are no significant gas gradients near the particle surface.

The most important effects considered in the model are particle drag and radiative and collisional heating/cooling of particles, and impact of particles on gas (two-way coupling). The following effects are not considered at this time: chemical reactions on the surface, processes that occur in liquid droplets (evaporation/condensation, coalescence), and particle phase change.

The most important features of the current implementation that distinguish it from [2] are as follows. The implementation (i) does not account for particle rotation: since particles in rocket plumes are largely spherical [9], particle rotation is considered unimportant, (ii) uses a statistical approach to calculate deflection angles of molecules on particle surface, (iii) gives flexibility of using arbitrary model of reflection of

molecules on particulates, and includes vibrational energy transfer in molecule-particle collisions, (iv) uses molecular fluxes and not the NTC scheme to calculate the number of molecule-particle collisions, (v) utilizes arbitrary inflow distribution of particles in terms of sizes and velocities, and (vi) employs different averaging strategy for particle force / energy transfer calculations.

3.1 Force and heat flux computation

The force F and heat flux Q on each particle exerted by gas molecules are calculated, similar to [3], as the sum over individual force and heat flux contributions of all surrounding molecules in a given cell,

$$\bar{F} = \int \bar{F}_\delta(\bar{c}) f(\bar{c}) d\bar{c}, \quad \bar{Q} = \int \bar{Q}_\delta(\bar{c}) f(\bar{c}) d\bar{c},$$

where $\bar{c} = \bar{u} - \bar{u}_p$, $\bar{u}$ is the molecular velocity vector, and $\bar{u}_p$ is the particle velocity vector. This is approximated by the summation over all molecules i in a cell at a given timestep,

$$\bar{F} \approx \sum_{i=1}^{N} \bar{F}_i(\bar{c}), \quad \bar{Q} \approx \sum_{i=1}^{N} \bar{Q}_i(\bar{c}).$$

It is also possible to compute the average force and heat flux over M consecutive time steps as,

$$\bar{F} \approx \frac{1}{M} \sum_{j=1}^{M} \sum_{i=1}^{N} \bar{F}_i(\bar{c}).$$

Introducing the momentum accommodation coefficient α_m and the translational, rotational, and vibrational energy accommodation coefficients α_t, α_r, and α_v, one can write the expression for the force per unit area,

$$\bar{F}_i = m \frac{F_{num}}{V_{cell}} \bar{c} \cdot$$

$$\cdot \left\{ (1 + \frac{4}{9}\alpha_m(1-\alpha_t))g + \alpha_m \alpha_t \frac{\sqrt{\pi}}{3} \sqrt{2\frac{k}{m}T_p} \right\},$$

where m is the molecular mass, F_{num} is the ratio of real to simulated molecules, V_{cell} is the cell volume, R_p is the particle radius, $g = |\bar{c}|$, and T_p is the particle temperature.

For the heat flux per unit area,

$$Q_i = \alpha_m \frac{F_{num}}{V_{cell}} g \Big\{ \alpha_t (\frac{1}{2} m g^2 - 2kT_p) +$$

$$\alpha_r (E_{rot} - \frac{\xi_{rot}}{2} kT_p) + \alpha_v (E_{vib} - \sum_v \frac{d\, k\, \theta_v}{\exp(\theta_v/T_p) - 1}) \Big\}.$$

Here, E_{rot} and E_{vib} are the molecular rotational and vibrational energies, ξ_{rot} is the number of rotational degrees of freedom, v denotes summation over vibrational modes, and d is the mode degeneracy.

Force and heat transfer computations use the average properties $\bar{u}$ and T_p for particulates that depend on particulate species, diameter, and spatial cell. Every time step the particle velocities are recalculated as follows,

$$\bar{v}(t + \Delta t) = \bar{v}(t) + \bar{F} \pi R_p^2 \Delta t / m_p,$$

where $\bar{v}$ and m_p are particulate velocity vector and mass. $\bar{F}$ is the force per unit area (see above) multiplied by the actual area of the particulate πR_p^2. Particle temperature is recalculated as

$$T(t + \Delta t) = T(t) + \Delta t \pi R_p^2 / (m_p C_p) Q +$$

$$\frac{3}{\rho_p R_p C_p} \sigma (T_{gas}^4 - T_p^4).$$

Here, C_p is the specific heat capacity of particulates, Q is the heat flux per unit area calculated at the previous step, σ is the Stefan-Boltzmann constant, and T_{gas} is the temperature of the surrounding gas (the cell temperature). The second term in the right hand side of the equation corresponds to the radiation gain or loss. Note that an emissivity of one is assumed here.

3.2 Two-way coupling

To account for the impact of particulates on gas, one needs to model the particle-molecule collision process. Two principal issues need to be addressed in this respect, (i) computation of the number of gas-particulate collisions, and (ii) modeling of each individual collision (change molecular velocities and energies).

The total number of collisions of gas molecules with a specific particle is calculated as the free-molecular number flux of molecules to the particle surface, which may be written as

$$N_c = \frac{n\bar{c}}{4} \pi D^2,$$

where n is the gas number density, c is the molecular velocity with respect to particle velocity, and D is particle diameter.

In this work, the majorant collision frequency [7] methodology has been applied, so that the number of majorant collisions is

$$N_{c,maj} = (\frac{n\bar{c}}{4} \pi D^2)_{max},$$

and the acceptance-rejection technique is used to select physical collisions.

Let us now describe the algorithm for molecule-particle collisions. It has two parts, (a) obtain the

point where molecule hits particle surface, and (b) perform reflection. In part (a) the surface reflection point is selecteded stochastically. After the reflection point is determined, the normal to the surface may found assuming that particles are spherical. Then, (b), new molecular states (velocities and internal energies) are calculated in the same way as for usual reflection of molecules on surfaces, and using specified accommodation coefficients. Note that molecular coordinates are not changed. The particle properties are not changed either since the impact of gas on particles is included through the momentum and heat flux modeling (see previous sections).

Part (b) is straightforward and therefore will not be described here. Part (a) consists of the following steps.

1. Calculate the reflection point in a local coordinate system. The local coordinate system is set so that the relative velocity vector is parallel to the X axis. The system is moving with the particle, so that the particle is still, and the molecule approaches with a negative velocity (see Fig. 1). The following approximation is used here,

$$R = R_{mol} + R_{part} \approx R_{part}.$$

The impact parameter b is selected randomly as

$$b = \sqrt{R_f} R.$$

The reflection point is initially located on XY plane, with its coordinates determined by a vector

$$x_0 = \begin{pmatrix} \sqrt{R^2 - b^2} \\ b \\ 0 \end{pmatrix}.$$

2. Rotate the reflection point around X axis at an angle $\phi = 2\pi R_f$, which will give the coordinate of the reflection point in the local coordinate system,

$$x_0 = Ax_0 = \begin{pmatrix} 1 & 0 & 0 \\ 0 & \cos\phi & -\sin\phi \\ 0 & \sin\phi & \cos\phi \end{pmatrix}$$

$$* \begin{pmatrix} \sqrt{R^2 - b^2} \\ b \\ 0 \end{pmatrix} = \begin{pmatrix} \sqrt{R^2 - b^2} \\ b\cos\phi \\ b\sin\phi \end{pmatrix}.$$

3. Transform the local (x_l) to the global coordinate system via the directional cosines,

$$\cos\alpha_1 \equiv \frac{Rg_x}{|g|}, \quad \cos\alpha_2 \equiv \frac{Rg_y}{|g|}, \quad \cos\alpha_3 \equiv \frac{Rg_z}{|g|}.$$

The equation of transformation is written as

$$x_g = Ex_l = \begin{pmatrix} e_{11} & e_{12} & e_{13} \\ e_{21} & e_{22} & e_{23} \\ e_{31} & e_{32} & e_{33} \end{pmatrix} * \begin{pmatrix} \sqrt{R^2 - b^2} \\ b\cos\phi \\ b\sin\phi \end{pmatrix}$$

where

$$e_{11} = v_x, \quad e_{12} = -v_y, \quad e_{13} = -v_z,$$

$$e_{21} = v_y, \quad e_{22} = \frac{v_z^2}{1+v_x} + v_x, \quad e_{23} = -\frac{v_y v_z}{1+v_x},$$

$$e_{31} = v_z, \quad e_{32} = -\frac{v_y v_z}{1+v_x}, \quad e_{33} = \frac{v_y^2}{1+v_x} + v_x.$$

4. Finally, the needed normal vector is determined by the following directional cosines,

$$\cos\psi_1 = e_{11}\sqrt{R^2 - b^2} + e_{12} b\cos\phi + e_{13} b\sin\phi,$$

$$\cos\psi_2 = e_{21}\sqrt{R^2 - b^2} + e_{22} b\cos\phi + e_{23} b\sin\phi,$$

$$\cos\psi_3 = e_{31}\sqrt{R^2 - b^2} + e_{32} b\cos\phi + e_{33} b\sin\phi.$$

4 Model Verification

Prior to being used to model complex 3D flows, the extended SMILE code has been extensively tested to verify its robustness and accuracy. An example of the verification is shown in Figs. 2 and 3 where the velocity and temperature of particulates introduced to a uniform gas stream are presented. The initial particulate temperature is 1000 K and velocity is 1000 m/s, and the corresponding gas properties are 2000 K and 2000 m/s. The gas and particle number densities are 10^{22}molecule/m^3 and 10^{12}molecule/m^3, respectively. Note that the obtained DSMC solution is in excellent agreement with the analytic solution.

5 Flow Conditions

The test case investigated in this work is a two-phase flow from a 130 N RCS aluminized propellant thruster into atmosphere at an altitude of 120 km. The thruster was located at a side of a small rocket that travels at a speed of 5 km/s and zero incidence. A conical nozzle was used with a throat diameter 1.6 cm, an exit diameter of 8.8 cm, and a half-angle of 15 deg. The alumina particle mass loading in the stagnation chamber was assumed to be 18%. The alumina particles were assumed to have a diameter of 3.6 μm that did not change in the simulations. The gas composition (mass fraction) at the nozzle throat was X[CO]=0.5186, X[HCl]=0.2559, X[N_2]=0.1170, X[H_2]=0.0479, X[H_2O]=0.0468, X[CO_2]=0.0138. The nozzle surface temperature was assumed to be 1000 K.

The rocket was modeled a blunted cone cylinder, and the thruster was positioned on the cylinder immediately after the cylinder-cone junction. The cone length was 1.73 m, and the cylinder length and thickness were 2.6 m and 0.4 m, respectively. The free stream temperature and number density were 354 K and 4.733 molecule/m^3, respectively. The free stream composition was X[N_2]=0.73, X[O]=0.18, X[O_2]=0.09. The reaction set used in this work was taken from [10].

6 Results and discussion

6.1 Flow Inside the Nozzle

The computations of the diverging part of the nozzle were performed using both VIPER and SMILE codes. The throat conditions obtained from the VIPER solution of the converging part of the nozzle were used in the DSMC modeling. Although over 10 million molecules and 3 million cells were used in the DSMC simulations, these numbers are about two orders of magnitude smaller than those required to strictly satisfy the corresponding requirements of the DSMC method (the throat-based Knudsen number is about $5 \cdot 10^{-5}$), and the DSMC results should therefore be considered as qualitative.

Comparison of the continuum and kinetic solutions is presented in Fig. 4, where the temperature fields are shown. Note that the DSMC computational domain was extended beyond the nozzle exit ($X = 0.1$ m). It is seen that there is a reasonable agreement between the two solutions, with the larger difference observed further from the nozzle centerline. The two solutions are close near the centerline. It is interesting to note that this is the region where all the particulates are concentrated. Relatively large mass of particulates results in their small divergence from the nozzle axis, as illustrated in Fig. 5. The blue colored region correspond to the part of the flow where no particulates was observed. The difference between the continuum and kinetic solutions is primarily attributed to different approaches to account for the drag force and heat flux on particles exerted by gas molecules (a continuum technique is used in the VIPER code, whereas the above free-molecule approach is utilized in SMILE).

The interaction between gas and particulates causes a drop in temperature of particulates, from 2,700 K at the throat to about 2,500 K at the nozzle exit. The change in particulate velocity is more pronounced, from about 700 m/s at the throat to about 1,200 m/s at the exit (see Fig. 6).

Another important fact established in the nozzle flow modeling, in addition to the concentration of particulates in the coreflow, is their visible deviation from the nozzle axis. This behavior is illustrated in Fig. 7, which shows that the density of particulates reaches its maximum values at some distance from the axis. This is attributed to the particulate transport inside the converging part of the nozzle, where the nonuniformity in particle concentration is created. Particles lag behind the gas flow in the converging part, and as the result move closer to the surface, and at the throat plane form a maximum located between the centerline and the surface.

At high particle loading values typical for aluminized propellant thruster, the gas influences the particulates, but the latter may also significantly impact the gas properties. In order to examine the interaction between gas and particulates, in addition to the baseline two-way coupling modeling the DSMC computations were also performed with a one-way coupling (particulates assumed not to affect the gas molecules). Comparison of the gas axial velocity fields for simulations with one-way and two-way coupling are presented in Fig. 8. Note a qualitative difference between these two cases. When the one-way coupling is included, the gas velocity inside the nozzle monotonically decreases with the radial distance from the nozzle centerline. The interaction with particulates that travel at lower speeds, though, results in a significant minimum in gas velocity. The velocity then increases at the nozzle axis due to the local minimum in particulate density in that region (see Fig. 7).

Lower gas velocities in the coreflow, in turn, result in lower particulate velocities for the two-way coupling case as compared to the one-way coupling, as shown in Fig. 9. The difference in the particulate velocities is significantly smaller, however, than for the gas velocities. At the nozzle throat it amounts to about 100 m/s, versus over 500 m/s for gas velocities.

One of the important parameters of the two-phase flow modeling is the particle size and mass. Although these parameters are relatively well known for aluminized propellant thrusters as compared to liquid propellant engines, there is still some uncertainty in particulate properties. To study the sensitivity of flow results to the particulate mass, a DSMC computation has also been performed for pure aluminum particles, whose mass is about 1.5 times smaller than for the baseline alumina case.

The general impact of the decrease in the mass of particles is their visibly larger divergence from the centerline due to a larger influence of the drag force. This effect is shown in Fig. 10 where the particle axial velocity fields are given for the two cases. Note also that aluminum particles accelerate to speeds up to 1,300 m/s at the nozzle exit versus about 1,200 m/s for alumina particles.

There is also a noticeable impact of the particle

mass on gas properties, illustrated in Fig. 11 for the axial velocity. As expected, the gas velocity in the region of particle-gas interaction is lower for the heavier particles. The particle-free region is not affected, though.

The gas-particle interaction may significantly impact the infrared radiation signatures, and one of the primary modeling issues is the accurate prediction of vibrational temperatures of different species. The main mechanism of influence of gas-particle collisions on vibrational temperature is the accommodation of vibrational energy on particulate surface. To examine the possible impact of vibrational energy accommodation, computations where performed for the complete (baseline) and no vibrational energy accommodation. The results for the vibrational temperature of one of the gas species are presented in Fig. 12. The computations show that the vibrational energy accommodation effect on vibrational temperature is relatively small, amounting to about 10% at the nozzle exit plane.

6.2 Modeling of the Plume Near Field

The macroparameters at the nozzle exit plane obtained with the VIPER code were used as the boundary condition for the plume near field calculations. The kinetic approach was employed for this stage, and about 4 million molecules and 2 million cells used in the computations have provided the required accuracy and resolution for the DSMC method. The computational domain extended 2.5 m downstream from the nozzle exit, where the plume is still dense enough to neglect the impact of the free stream on the coreflow. Only plume species have therefore been considered in the simulation, with no chemical reactions included.

Although this stage has been used primarily to provide a starting surface for the subsequent 3D computations, it has also allowed us to examine the impact of the two-way coupling that has been previously shown important for the flow inside the nozzle. The gas axial velocity profiles are given in Fig 13 for the one-way and two-way coupling cases. Note that the nozzle exit plane is located at X=0.1 m. As expected, there is no visible impact of particulates on gas in the particle-free regions of the plume. In the coreflow, where the concentration of particles is considerable, the two-way coupling results in a decrease of gas velocities by a few percent.

Although the influence of gas-particle collisions on gas is smaller in the plume than inside the nozzle, this effect is still noticeable, and is most pronounced for the gas translational temperature fields (see Fig. 14). The difference originates in the first few centimeters downstream from the nozzle exit, where the concentration of particulates is maximum.

The influence of two-way coupling on particulate properties is very small, and the particle flow fields obtained by one-way and two-way coupling are practically identical. The particle temperature field in the plume near field is shown in Fig. 15. It is seen that the particle temperature decreases downstream; this decrease is attributed to the radiative cooling and not the gas-particle collisions. The computation with the radiative cooling turned off has shown no visible change in particle temperature. The computations also showed that the particle velocities do not change along the stream lines, proving therefore that the influence of the particle drag in the nearfield is negligible.

6.3 Plume-Atmosphere Interaction

The 3D modeling of the plume-atmosphere interaction was performed with the SMILE code using a starting surface obtained using the plume near field solution described in the previous section. The starting surface was generated along the density isoline with a value of $2 \cdot 10^{21}$ kg/m^3; it expands about 0.45 m downstream from the nozzle exit. An elliptic distribution function was used for the plume molecules that enter the computational domain from that starting surface. The size of the computational domain is 10.4 m in the X direction, 7.4 m in the Y direction, and 2.6 m in the Z direction (a symmetry plane was used at Z=0). Here, X coincide with the plume axis, and Y is parallel to the free stream vector. A total of about 10 million simulated molecules and 5 million collision cells was used in the 3D computations.

The sensitivity studies have shown that the impact of gas-particle collisions is negligibly small, and both gas and particle flow fields for one-way and two-way coupling are identical. Particle speed is practically constant at 1,350 m/s, and does not change with distance from the nozzle. Particle temperature decreases only due to the radiation cooling. When the radiation cooling is turned off, it stays at about 2,300 K throughout the plume. This is illustrated in Fig. 16, where the particle temperature with and without the radiation cooling is shown in XY plane. Note here that the effect of this cooling on gas molecules has not been incorporated in the present model, and may have some impact on gas properties.

The distribution of particle number density in XY plane is presented in Fig. 17. Similar to the flow inside the nozzle, at each axial station downstream from the nozzle exit, the particle density has a maximum off the nozzle centerline, which is related to the above mentioned fact that inside the converging part of the nozzle particles concentrate in the regions close to the surface. Note also that at about 10 m downstream from the nozzle exit, the particle density drops over

three orders of magnitude, proportionally decreasing the collision rate of gas molecules with particulates.

This is illustrated in Fig. 19, where the mean free path of gas molecules between collisions with particles is shown. The mean free path sharply increases with distance from the nozzle, and reaches about 3 km at 9 m downstream from the nozzle exit.

Let us now consider the possibility of the interaction of high-speed free stream molecules with plume particulates. The number density of the free stream nitrogen is presented in Fig. 19. It is clear that the plume number density in the first 9 m from the nozzle exit is too high for free stream molecules to penetrate to the nozzle centerline. There is a weak shock observed at the wind side of the plume, formed by the free stream molecules, with the density almost three times as high as in the free stream, but there are no free stream molecules in the plume core flow where the particles reside (compare with Fig. 18). For distances along the nozzle centerline larger than considered, the collisions between the free stream and plume particulates may occur, but the particulate density is expected to be too small for these collisions to have a significant effect.

Figures 20 and 21 show the total gas number density and translational temperature, respectively. The impact of particulates is visible in the coreflow. As expected, the maximum of translational temperature is observed in the plume-atmosphere interaction region. There is also a small local maximum at the nozzle axis due to gas-particle interaction inside the nozzle and in a small vicinity downstream from the nozzle exit. The computations also showed that with the complete vibrational energy accommodation the vibrational temperature of the plume species is about 1,500 K in the plume coreflow, and about 1,000 K in the particle free regions of the plume and in the plume-interaction regions.

7 Conclusions

Numerical investigation of a two-phase plume from a small side thruster interacting with atmosphere at 120 km was performed using a combined continuum-kinetic approach. The solution of Navier-Stokes equations inside the nozzle was used to specify a starting surface for a 2D DSMC computation of the plume near field, that was then used for a subsequent 3D DSMC computation of the plume-atmosphere interaction region. The details of the DSMC implementation of the two-way gas-particulate coupling are presented. The current implementation uses molecular fluxes to calculate the number of gas-particulate collisions, and is based on a statistical approach to calculate deflection angles.

The study of sensitivity of computational results to various parameters of the approach has been performed. It was found that

- For small thrusters, accurate modeling of particulates inside the converging part of the nozzle is critical since it practically determines the particle divergence from the nozzle axis inside the plume
- The interaction between gas and particulates (two-way coupling) has an important effect on the flow in the diverging part of the nozzle
- Particles are concentrated in the coreflow, and the divergence angle of particulates from the nozzle centerline is about 6 deg
- The kinetic and continuum solutions of the flow inside the nozzle are in reasonable agreement in terms of gas as well as particulate properties
- A 40 percent reduction in particle mass increases the divergence angle in the diverging part of the nozzle by a factor of two
- Accommodation of vibrational energy of gas molecules at the particulate surface has little effect on vibrational temperature
- The two-way coupling has negligible impact on the flow after a few centimeters from the nozzle exit
- Particle velocities do not change noticeably after the nozzle exit; particle temperature in the plume decreases only due to radiative cooling
- There is no interaction between the free stream molecules and particulates in the first ten meters from the nozzle exit; little effect is expected from this interaction in the far field of the plume.

8 Acknowledgment

This work was supported by the Air Force Office of Scientific Research and the Air Force Research Laboratory Propulsion Directorate under Contract No. F04611-99-C-0025.

References

[1] York B., Lee R., Sinha, N., Dash, S. "Progress in the simulation of particulate interactions in solid propellant rocket exhausts'," AIAA Paper 2001-3590.

[2] Burt, J.M., Boyd, I.D. "Development of a two-way coupled model for two-phase rarefied flows," AIAA Paper 2004-1351.

[3] Gallis, M.A., Torczynski, J.R., Rader, D.J. "An approach for simulating the transport of spherical particles in a rarefied gas flow via the direct simulation Monte Carlo method," Physics of Fluids, Vol. 13, No. 11, 2001, pp. 3482-3492.

[4] Anonymous, "Viscous Interaction Performance Evaluation Routine for Two-Phase Nozzle Flows with Finite Rate Chemistry, Viper 3.6 User's Guide," Software and Engineering Associates, Inc., Carson City, NV, 2003.

[5] Kawasaki, A. H., Coats, D. E., Berker, D. R., "A Two-Phase, Two-Dimensional, Reacting Parabolized Navier-Stokes Sover for the Prediction of Solid Rocket Moter Flowfields," AIAA Paper 92-3600.

[6] Ivanov , M.S., Markelov, G.N., and Gimelshein S.F. "Statistical simulation of reactive rarefied flows:numerical approach and applications," AIAA Paper 98-2669.

[7] Ivanov, M.S., Rogasinsky, S.V., "Analysis of the numerical techniques of the direct simulation Monte Carlo method in the rarefied gas dynamics," *Soviet J. Numer. Anal. Math. Modeling*, Vol. 3, No. 6, 1988, pp. 453-465.

[8] Bird, G.A., "Monte-Carlo simulation in an engineering context," *Rarefied Gas Dynamics,* edited by S. Fisher, Vol. 74, Progress in Astronautics and Aeronautics, 1981, pp. 239-255.

[9] Simmons, F.S. *Rocket exhaust plume phenomenology.* The Aerospace Press, 2000.

[10] Gimelshein S.F., Levin D.A., Alexeenko A.A. "Modeling of chemically reacting flows from a side jet at high altitudes," *Journal of Spacecraft and Rockets,* 2004, Vol. 41, No. 4, pp. 582-591.

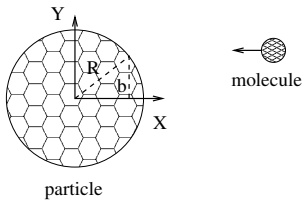

Figure 1: Particle-molecule collision in the local coordinate system.

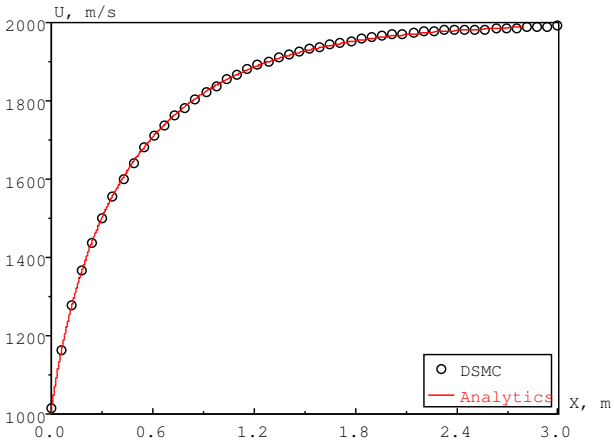

Figure 2: Velocity distribution of particles introduced in uniform gas flow.

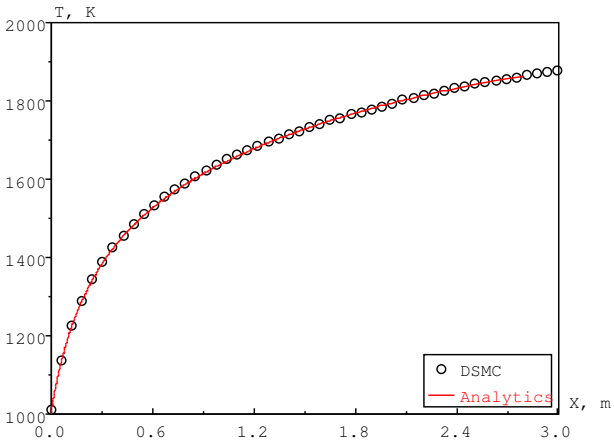

Figure 3: Surface temperature distribution of particles introduced in uniform gas flow.

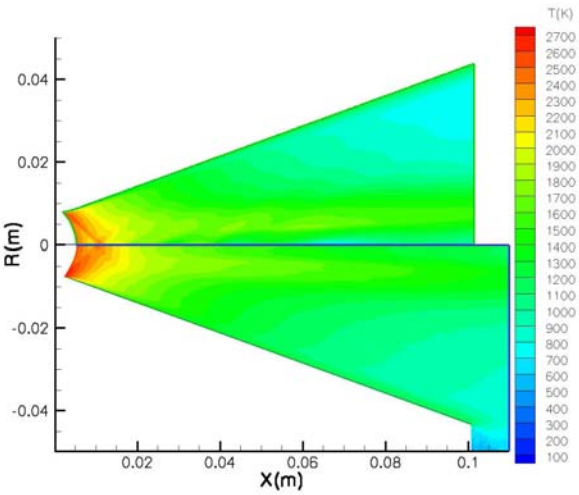

Figure 4: Gas overall temperature (K) field inside the nozzle obtained with the continuum (top) and kinetic (bottom) approaches.

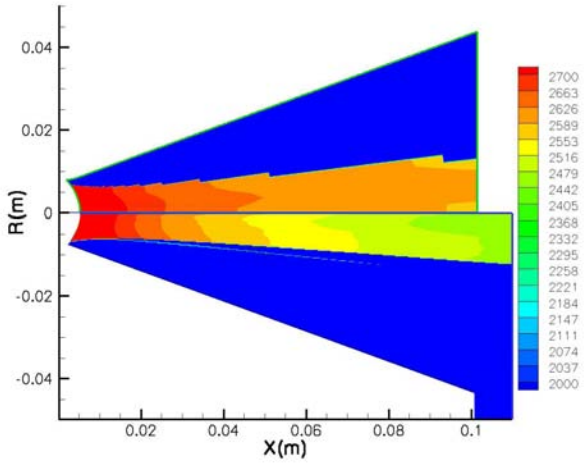

Figure 5: Particle temperature (K) field inside the nozzle obtained with the continuum (top) and kinetic (bottom) approaches.

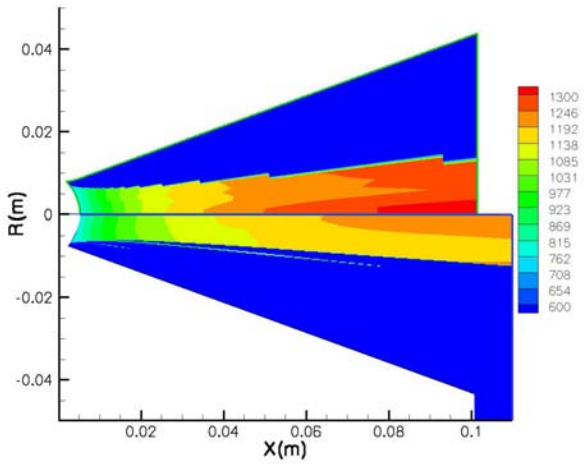

Figure 6: Particle axial velocity (m/s) field inside the nozzle obtained with the continuum (top) and kinetic (bottom) approaches.

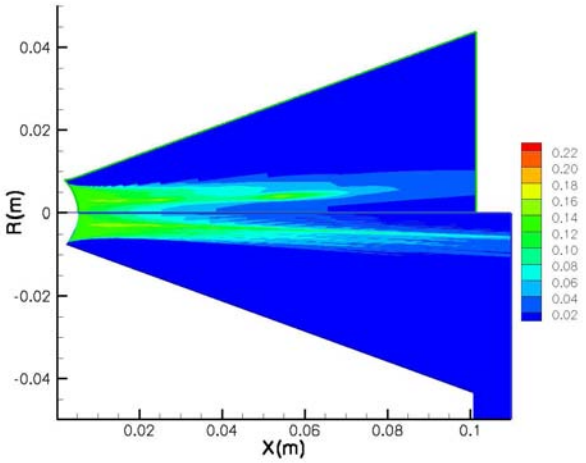

Figure 7: Particle density (kg/m^3) field inside the nozzle obtained with the continuum (top) and kinetic (bottom) approaches.

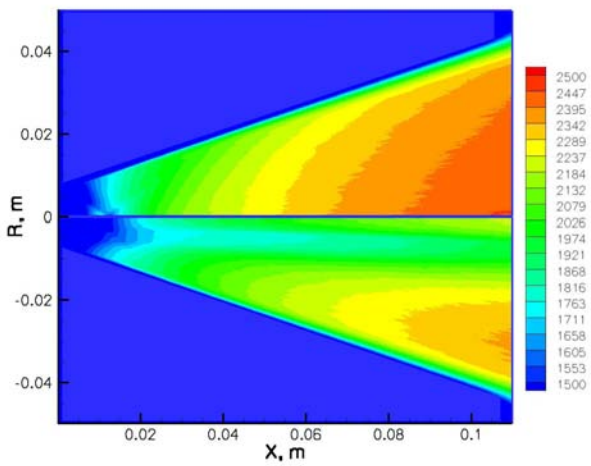

Figure 8: Impact of two-way coupling on gas axial velocity (m/s) inside the nozzle. Top, one-way coupling; bottom, two-way coupling.

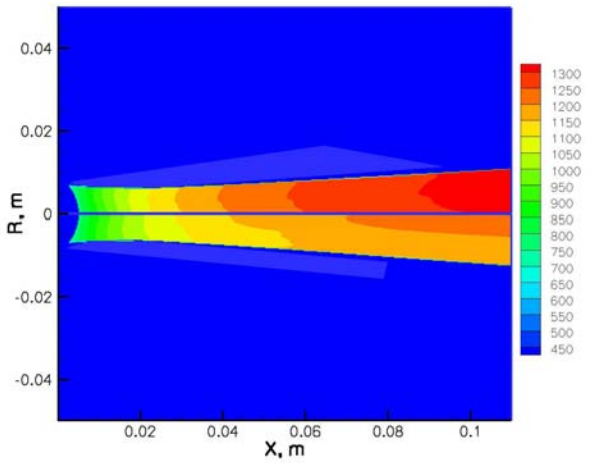

Figure 9: Impact of two-way coupling on particle axial velocity (m/s) inside the nozzle. Top, one-way coupling; bottom, two-way coupling.

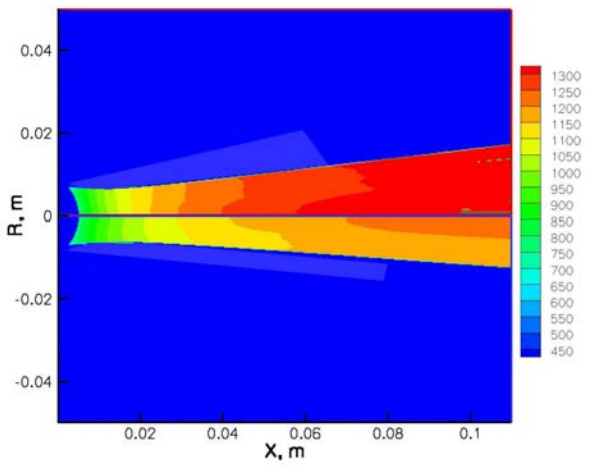

Figure 10: Impact of particle mass on particle axial velocity (m/s) inside the nozzle. Top, aluminum particles; bottom, alumina particles.

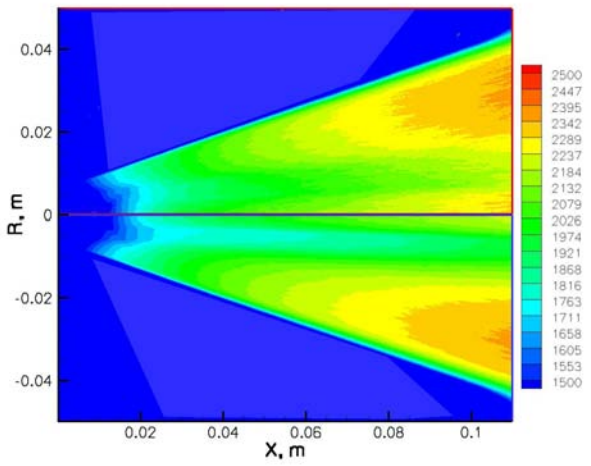

Figure 11: Impact of particle mass on gas axial velocity (m/s) inside the nozzle. Top, aluminum particles; bottom, alumina particles.

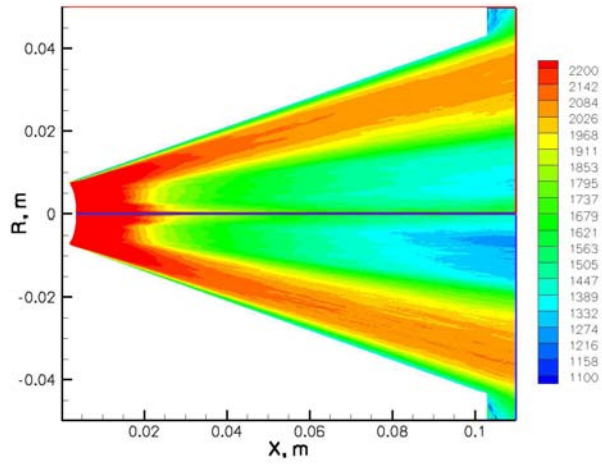

Figure 12: CO vibrational temperature (K) inside the nozzle for different vibrational energy accommodation coefficients on particle surface. Top, full accommodation; bottom, no accommodation

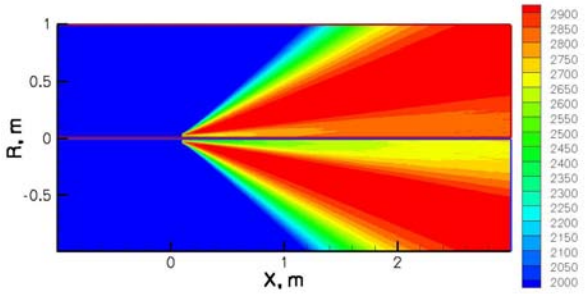

Figure 13: Impact of two-way coupling on gas axial velocity (m/s) in the plume near field. Top, one-way coupling; bottom, two-way coupling.

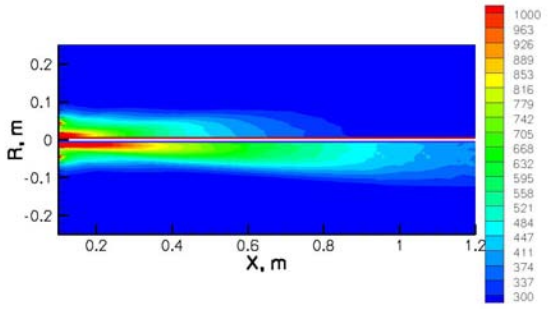

Figure 14: Impact of two-way coupling on gas translational temperature (K) in the plume near field. Top, one-way coupling; bottom, two-way coupling.

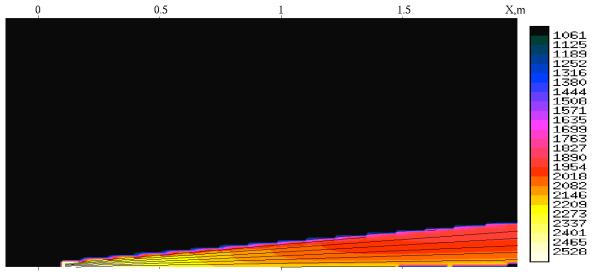

Figure 15: Particle temperature (K) and streamlines in the plume near field.

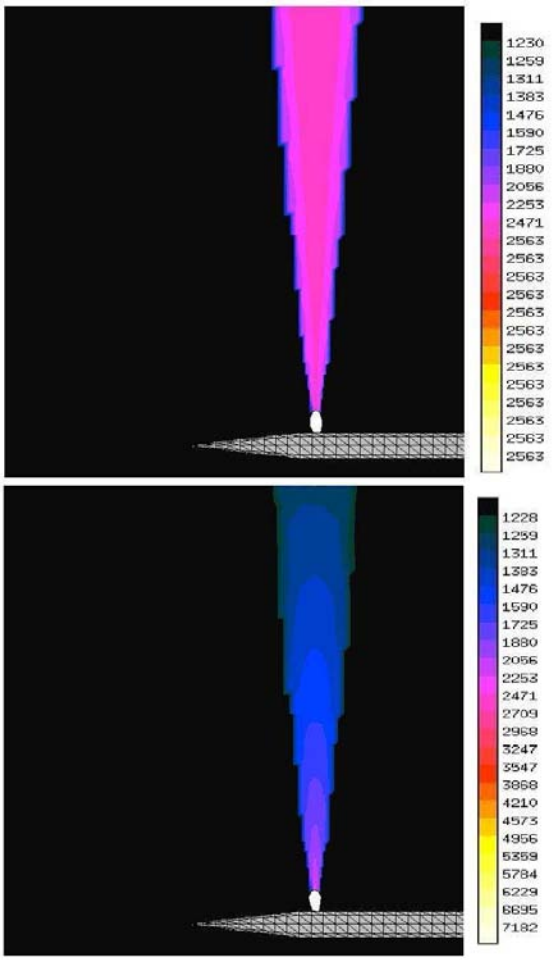

Figure 16: Particle temperature (K) in the plume-atmosphere interaction region with radiation cooling turned off (top) and on (bottom). Here, white region shows the location of the starting surface for 3D modeling

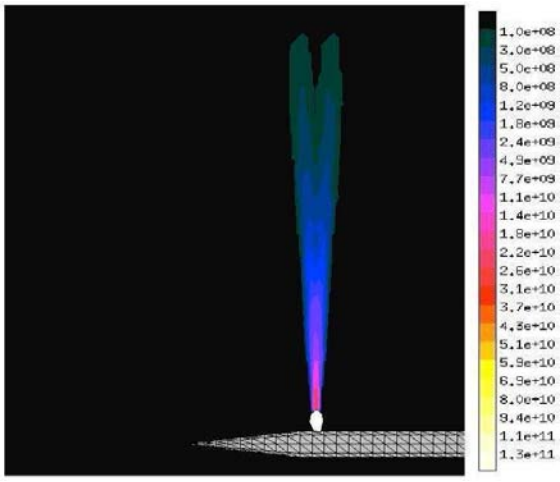

Figure 17: Particle number density ($1/m^3$) in the plume-atmosphere interaction region.

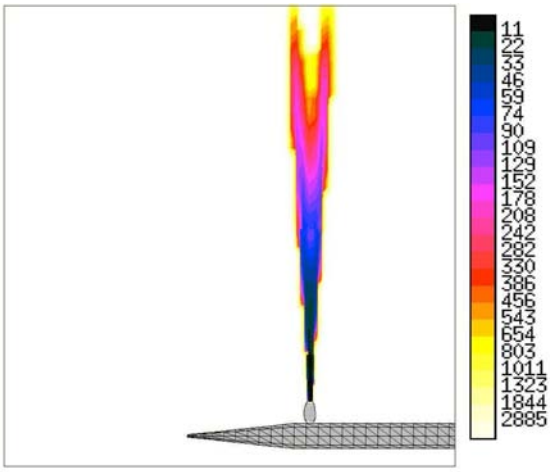

Figure 18: Gas mean free path between collisions with particles (m) in the plume-atmosphere interaction region.

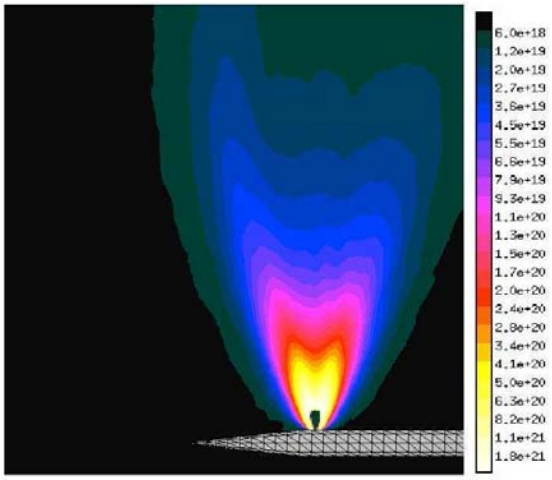

Figure 20: Gas number density ($1/m^3$) in the plume-atmosphere interaction region.

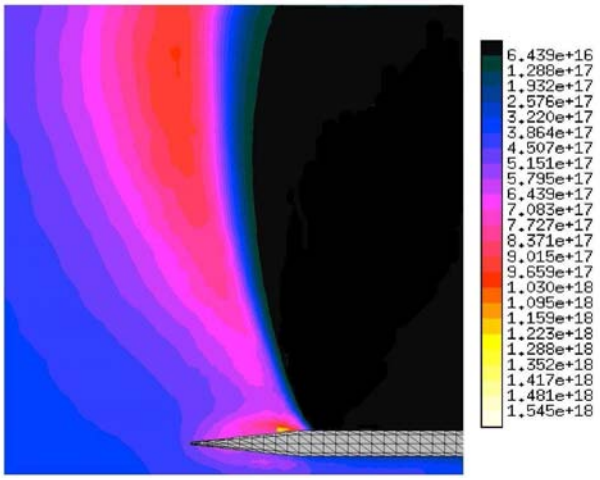

Figure 19: Free stream nitrogen number density ($1/m^3$) in the plume-atmosphere interaction region.

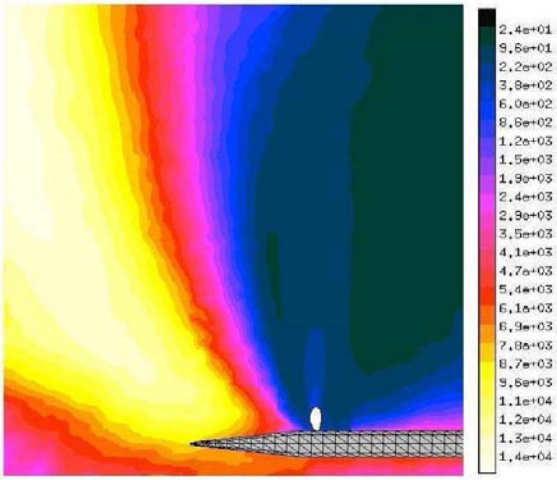

Figure 21: Gas translational temperature (K) in the plume-atmosphere interaction region.